Sensor Data Fusion using Kalman Filter for LAPAN-A2 Satellite Attitude Estimation

Shabri C. AKMAL*,[1], Ridanto Eko POETRO[1], Javensius SEMBIRING[1], Satriya UTAMA[2]

*Corresponding author
[1]Aerospace Engineering, Faculty of Mechanical and Aerospace Engineering,
Bandung Institute of Technology,
Ganesha St. 10, Bandung 40132, Indonesia,
shabriakmal@gmail.com*
[2]Research Centre for Satellite Technology,
National Research and Innovation Agency,
Bogor 16310, Indonesia

DOI: 10.13111/2066-8201.2023.15.4.1

Received: 11 October 2023/ Accepted: 15 November 2023/ Published: December 2023

Abstract: *LAPAN A2 is a Low Earth Orbit (LEO) satellite with the primary mission to monitor the area. In order to fulfil the mission's objectives, the Satellite attitude must be controlled properly. One of the control processes under consideration is the output attitude estimation. Attitude estimation processes in satellites mostly use satellite sensor output transformation. The estimation process, however, cannot be carried out with only one sensor where the generated transformation does not represent the satellite actual attitude. Thus, a fusion of two or more attitude sensors is needed. However, measurement noise, such as the effect of the Earth's albedo on the sun sensor and the interference of the Earth's magnetic field on the magnetometer, is incorporated into the estimation process. Thus, a filtering process is needed. Hence, this study aims to investigate the utilization of the sensor output raw data fusion combined with the Kalman Filter algorithm to estimate the LAPAN-A2 satellite attitude in the form of Euler angle.*

Key Words: *LAPAN A2, Attitude Estimation, Sensor Data Fusion, Kalman Filter*

1 INTRODUCTION

Satellite development has become a vital part of the digital era, and for more proper design development, it has become a research area in an educational curriculum. Beyond the purely educational realm, the satellite development brings benefits in the areas of technology development and scientific objectives.

The National Research and Innovation Agency, Jakarta, Indonesia and the Amateur Radio Organization of Indonesia (ORARI), Jakarta, Indonesia have been developing the micro-satellite LAPAN-A2/ORARI Satellite. This satellite has a mass of about 74 kg and a dimension of 47 cm ×50 cm ×36 cm [1]. It was launched on September 28, 2015, as a secondary payload to ISRO's AstroSat spacecraft.

The launch site was SDSC (Satish Dhawan Space Center) in India, and the launch vehicle was PSLV-C30 [2]. LAPAN-A2 primary mission is to provide actual, frequent, and accurate

data for disaster mitigation communication, equatorial maritime monitoring, and Indonesian land use, natural resources, and environmental monitoring [1].

In order to be able to fulfil the mission objectives, LAPAN-A2 has been operated in a near equatorial circular orbit with an altitude of about 650 km (LEO), and an inclination of 60. For this mission, near equatorial orbit will be used fourteen times per day (day and night) for approximately eleven minutes on average [1].

LAPAN-A2 attitude must be controlled because of its limited time to communicate with the ground station and its earth-pointing maneuver for monitoring purposes. The sensors, which consist of a sun sensor, magnetometer, star sensor, and gyroscope, must accurately estimate the satellite attitude in order to provide the optimal estimation attitude for controlling the satellite's attitude.

However, noise disturbances in the Earth's magnetic field cause inaccuracies in the magnetic field measurement by magnetometer [3], and the sun eclipse incident causes dark areas where the sun sensor cannot provide a measurement output [4]. Moreover, daytime operation where the star sensor is exposed to the sun exposure means that the star sensor cannot be properly operated as the main attitude sensor of the satellite [5]. These events in singular sensor utilization cause errors in attitude estimation.

In addition to the phenomena mentioned, the transformation matrix generated from the output of one sensor produces many solutions [6, 7], while the solution required is only one solution at a time. Thus, a fusion of two or more sensors is required in the estimation method. The combination of sensors used in general is a sun sensor, magnetometer, and gyroscope [4, 5, 8, 9]. Other combination such as magnetometer and gyroscope [3] was also done but it did not get better accuracy.

Estimation methods that can be used for this process are TRIAD [10, 11], the Davenport q-method [12], and the SVD method [13]. However, the Davenport q-method and the SVD method are fine methods that require a long time to complete the estimation process [3], so it is contrary to the research objective to find a fast method due to the limited contact time of the satellite with the ground station.

The solution resulting from the TRIAD, however, is still bound by the errors resulting from the measurement as mentioned in the SERPENS II [8] and LAPAN A2 [11] missions.

So, the error filtering process needs to be done using the Kalman filter method [4, 5, 8, 9]. Moreover, the filtering method has never been carried out on the LAPAN-A2 satellite [11].

Therefore, this study aims to investigate the performance of the attitude estimation model by fusing the sensor raw data output from the sun sensor and magnetometer on the LAPAN-A2 satellite. The estimation model will be carried out using the TRIAD algorithm model, and its performance will be improved using the Extended Kalman Filter method.

The output data from the gyroscope will be used in the filtering method as a predictive model. The results of the estimation method will be the Euler angle from the LAPAN-A2 satellite and will be compared with the output from the star sensor as an assumption of the actual attitude value.

2. SENSOR MEASUREMENT

In previous research [4, 5, 8, 9], the combination of sensors used was a sun sensor, a magnetometer, and a gyroscope.

This section will explain a little how the sensors work and its specifications on the LAPAN-A2 satellite. It will also be explained about the star sensor as a comparison sensor. Table 1 summarizes the specifications of these sensors.

Table 1. LAPAN-A2 Sensors Spefication

Sensor	Type	Specification
Sun Sensor	Coarse Sun Sensor (CSS)	Sensor with readings from solar panel current output (in mA)
Magnetometer	Three Axis Magnetometer	Field range: $+/- \ 6 \times 10^4 \ (nT)$ Accuracy: $2 \times 10^4 \ (nT)$ Power consumption: 1 W
Gyroscope	Laser Gyro	Bias stability: ≤ 2º/h Random walk: ≤ 0.6º/h$^{1/2}$ Power consumption: ≤ 2.3 W
Star Sensor	Charged Coupled Device (CCD)	FOV: 31º x 31º Update period: 5 Hz Power consumption: 3 W
	Complementary Metal Oxide Semiconductor (CMOS)	FOV: 14º x 14º Update period: 4 Hz Power consumption: 2.5 W

The sun sensor on the LAPAN-A2 satellite is Coarse Sun Sensor (CSS) where solar cell panels are installed on six satellite sides. The six solar panels will change the light received into an electric current (in mili Ampere (mA)). The current value output from each side of the satellite is compared with each other to find the sun vector direction in the satellite (body) coordinate frame, $\vec{\boldsymbol{X}}^{\mathrm{B}}_{\mathrm{sun}}$. Although the same axis indicates positive and negative current value readings, the larger current value on the same axis comes from the sun, while the smaller one comes from the Earth's albedo. The larger value will be used as the current value reading on the axis [11].

While for the magnetometer, the LAPAN-A2 satellite uses a Magnetic Field Sensor (MFS). This sensor will measure the direction of the earth's magnetic field vector at the satellite's position at that time, $\vec{\boldsymbol{B}}^{\mathrm{mag}}$. The output of this sensor is magnetic field strength (in nano Tesla (nT)). in the magnetometer coordinate frame [1].

The outputs from the two sensors have different coordinate frames and these outputs for the estimation process must be fused by converting the coordinate frames and outputs. For that, the output from the magnetometer must be converted into a satellite coordinate frame.

Meanwhile, for the output of the two sensors, only the direction is taken for the calculation of attitude estimation by normalizing the output vectors of the two sensors which are already in the satellite coordinate frame.

The normalization process can be seen in the equation (1) and (2).

$$\hat{\boldsymbol{x}}^{\mathrm{B}}_{\mathrm{sun}} = \frac{\vec{\boldsymbol{X}}^{\mathrm{B}}_{\mathrm{sun}}}{\left\|\vec{\boldsymbol{X}}^{\mathrm{B}}_{\mathrm{sun}}\right\|} \tag{1}$$

$$\hat{\boldsymbol{x}}^{B}_{mag} = \frac{\left(\boldsymbol{R}^{\mathrm{B}}_{\mathrm{mag}}\,\vec{\boldsymbol{B}}^{\mathrm{mag}}\right)}{\left\|\boldsymbol{R}^{\mathrm{B}}_{\mathrm{mag}}\,\vec{\boldsymbol{B}}^{\mathrm{mag}}\right\|} \tag{2}$$

With $\boldsymbol{R}^{\mathrm{B}}_{\mathrm{mag}}$ is the rotation matrix from magnetometer coordinate to satellite (body) coordinate frame. The LAPAN-A2 satellite employs a ring laser gyroscope (RLG) for its gyroscope [1]. This sensor utilizes the properties of light to measure the angular velocity vector of the satellite in inertial space, $\vec{\boldsymbol{\omega}}^{\mathrm{B}}_{\mathrm{I}}$. The angular velocity vector obtained from the gyroscope, when integrated, will obtain a change in the angle of the satellite every time. To get the angle, the gyroscope needs to get information about the initial angle of the satellite from other sensors. Coupled with the noise in the angular velocity measurement, the gyroscope angle

measurement can only be called a predictive measurement and needs to be corrected by other sensor calculations at any given time. Therefore, the gyroscope measurement will be used as a predictive state in the Kalman Filter process. The star sensor on the LAPAN-A2 satellite uses complementary metal oxide semiconductors (CMOS) and charged coupled devices (CCDs) to scan the sky and gather data on the positions of stars. Any movement of the vehicle will be visible as a shifting of the stars in the field of view. When projected onto two planes that are perpendicular to one another and contain the sensor boresight axis, a star camera measures the elevation of the line of sight to a star. To estimate the camera attitude relative to an inertial frame of reference, there or more stars locations on the sensor and their locations in inertial coordinates are required. The captured star image will form a certain pattern which will be matched with the database on the sensor to estimate the sensor attitude in the inertial frame. Because the star sensor calculates the brightness magnitude of the star to form a pattern, the star sensor will be sensitive to light disturbances. Observation during the day where the sensor is exposed to sunlight is not recommended. Therefore, in this research the star sensor will be used as a comparison of the attitude estimation results obtained.

3. COORDINATE REFERENCE FRAME

In this section, the coordinate reference frames used in the research are: Earth Centered Inertial (ECI), Earth Centered Earth Fixed (ECEF), North – East – Down (NED), orbital frame, satellite body frame [14], and magnetometer coordinate frame [15] as addition. The illustration of coordinate reference frame can be seen in Fig. 1 – 5.

ECI Earth Centered Inertial (ECI) is a coordinate frame that has its origins at the center of mass of the Earth and is fixed with respect to the stars. For objects in space, the equations of motion that describe the orbital motion are simpler in a non-rotating frame such as ECI. The X-axis in the ECI coordinate frame points to the vernal equinox, the Z-axis to the North Pole, and the Y-axis is in the equatorial plane according to the right-hand rule.

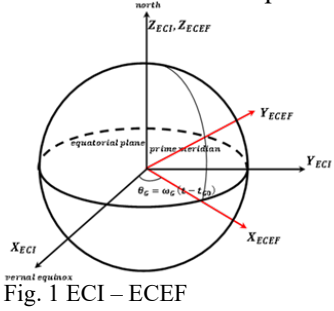

Fig. 1 ECI – ECEF Transformation Illustration

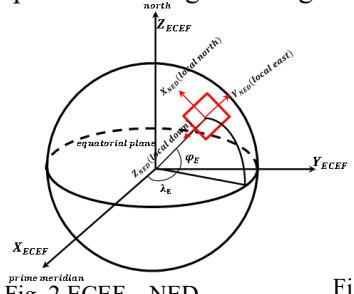

Fig. 2 ECEF – NED Transformation Illustration

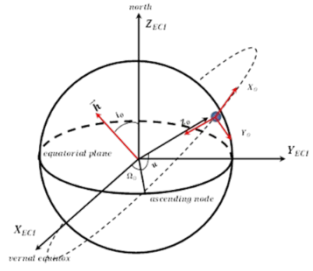

Fig. 3 ECI – Orbital Coordinate Frame Transformation Illustration

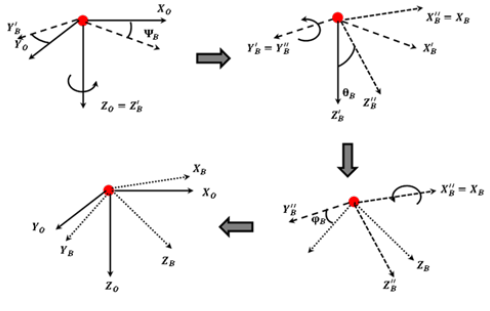

Fig. 4 Orbital–Body Coordinate Frame Transformation Illustration

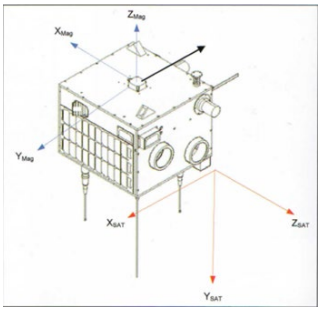

Fig. 5 Magnetometer –Body Coordinate Frame in LAPAN-A2 Illustration

ECEF Earth Centered Earth Fixed (ECEF) is a coordinate frame where the X-axis is in the equatorial plane and always points to the prime meridian, which is at 0 degree of logitude, the Z-axis always points to the north pole, and the Y-axis is in the equatorial plane following the right-hand rule. ECEF frame can be formed by rotating coordinate in the Z_{ECI} by the same amount as the Greenwich Hour Angle, θ_G. ECEF coordinate illustration can be seen in Figure 1. The transformation matrix from the ECI coordinate frame to the ECEF coordinate frame, $\boldsymbol{R}_{\mathrm{I}}^{\mathrm{E}}$, based on Figure 1 can be formed as equation (3) and (4).

$$\boldsymbol{R}_{\mathrm{I}}^{\mathrm{E}} = R_{\mathrm{z}}(\theta_{\mathrm{G}}) = \begin{bmatrix} \cos\theta_{\mathrm{G}} & \sin\theta_{\mathrm{G}} & 0 \\ -\sin\theta_{\mathrm{G}} & \cos\theta_{\mathrm{G}} & 0 \\ 0 & 0 & 1 \end{bmatrix} \tag{3}$$

where

$$\theta_{\mathrm{G}} = \omega_{\mathrm{G}}\,(t - t_{G0}) \tag{4}$$

with θ_G = Greenwich Hour Angle (rad), ω_G = Greenwich Point Angular Rate (Earth Angular Momentum) (rad/s), t_{G0} = time reference when greenwich point meet vernal equinox (s), and t = object time (s).

NED North – East – Down is a spatial reference system based on the tangent plane defined by the local vertical direction and the Earth's axis of rotation. In the NED frame, the X-axis will point to local north, the Y-axis will point to local east, and the Z-axis will be perpendicular to the local plane following the right-hand rule. NED can be formed from by rotating the Z_{ECEF} by the same amount as the local earth longitude, λ_{E}, then rotating in the new Y-axis to north pole by the same amount as the local earth latitude, φ_{E}, and rotating 270^0 to the new Y-axis. The NED coordinate frame illustration can be seen in Figure 2. The transformation matrix from the ECEF coordinate frame to the NED coordinate frame, $\boldsymbol{R}_{\mathrm{E}}^{\mathrm{N}}$, based on Figure 2 can be formed as equation (5).

$$\begin{aligned} \boldsymbol{R}_{\mathrm{E}}^{\mathrm{N}} = \boldsymbol{R}_{\mathrm{y}}(270^0)\boldsymbol{R}_{\mathrm{y}}(-\varphi_E)\boldsymbol{R}_{\mathrm{z}}(\lambda_E) &= \begin{bmatrix} 0 & 0 & 1 \\ 0 & 1 & 0 \\ -1 & 0 & 0 \end{bmatrix}\begin{bmatrix} \cos\varphi_{\mathrm{E}} & 0 & \sin\varphi_{\mathrm{E}} \\ 0 & 1 & 0 \\ -\sin\varphi_{\mathrm{E}} & 0 & \cos\varphi_{\mathrm{E}} \end{bmatrix}\begin{bmatrix} \cos\lambda_{\mathrm{E}} & \sin\lambda_{\mathrm{E}} & 0 \\ -\sin\lambda_{\mathrm{E}} & \cos\lambda_{\mathrm{E}} & 0 \\ 0 & 0 & 1 \end{bmatrix} \\ &= \begin{bmatrix} -\sin\varphi_{\mathrm{E}}\cos\lambda_{\mathrm{E}} & -\sin\varphi_{\mathrm{E}}\sin\lambda_{\mathrm{E}} & \cos\varphi_{\mathrm{E}} \\ -\sin\lambda_{\mathrm{E}} & -\cos\lambda_{\mathrm{E}} & 0 \\ -\cos\varphi_{\mathrm{E}}\cos\lambda_{\mathrm{E}} & -\cos\varphi_{\mathrm{E}}\sin\lambda_{\mathrm{E}} & -\sin\varphi_{\mathrm{E}} \end{bmatrix} \end{aligned} \tag{5}$$

Orbital. An orbital coordinate frame is a coordinate frame where the X-axis is parallel with the satellite velocity vector and tangent to the orbital plane, the Z-axis always points to the center of mass, and the Y-axis is perpendicular to the orbital plane and in the opposite direction to the orbital angular momentum vector. An Orbital frame can be formed by rotating in the Z_{ECI} by the same amount as the orbital right ascension angle, Ω_{O}, then rotating in the new X-axis to equatorial plane by the same amount as the orbital inclination angle, i_o and rotating about orbital angular momentum by the same amount as the u angle which is addition product of orbital argument perigee, ω_{O}, and orbital true anomaly, θ_{O}, then followed by rotating 90^0 in the new Z-axis and rotating 270^0 to the new X-axis. The orbital coordinate frame illustration can be seen in Figure 3. The transformation matrix from the ECI coordinate frame to the orbital coordinate frame, $\boldsymbol{R}_{\mathrm{I}}^{\mathrm{O}}$, can be formed as equation (6) and (7).

$$\begin{aligned} \boldsymbol{R}_{\mathrm{I}}^{\mathrm{O}} &= R_{\mathrm{x}}(270^0)R_{\mathrm{z}}(90^0)R_{\mathrm{z}}(\mathrm{u})R_{\mathrm{x}}(\mathrm{i_O})R_{\mathrm{z}}(\Omega_{\mathrm{O}}) \\ &= \begin{bmatrix} 1 & 0 & 0 \\ 0 & 0 & -1 \\ 0 & 1 & 0 \end{bmatrix}\begin{bmatrix} 0 & 1 & 0 \\ -1 & 0 & 0 \\ 0 & 0 & 1 \end{bmatrix}\begin{bmatrix} \cos\mathrm{u} & \sin\mathrm{u} & 0 \\ -\sin\mathrm{u} & \cos\mathrm{u} & 0 \\ 0 & 0 & 1 \end{bmatrix}\begin{bmatrix} 1 & 0 & 0 \\ 0 & \cos\mathrm{i_O} & \sin\mathrm{i_O} \\ 0 & -\sin\mathrm{i_O} & \cos\mathrm{i_O} \end{bmatrix}\begin{bmatrix} \cos\Omega_{\mathrm{O}} & \sin\Omega_{\mathrm{O}} & 0 \\ -\sin\Omega_{\mathrm{O}} & \cos\Omega_{\mathrm{O}} & 0 \\ 0 & 0 & 1 \end{bmatrix} \\ &= \begin{bmatrix} -\sin\mathrm{u}\cos\Omega_{\mathrm{O}} - \cos\mathrm{u}\cos\mathrm{i_O}\sin\Omega_{\mathrm{O}} & -\sin\mathrm{u}\sin\Omega_{\mathrm{O}} + \cos\mathrm{u}\cos\mathrm{i_O}\cos\Omega_{\mathrm{O}} & \cos\mathrm{u}\sin\mathrm{i_O} \\ -\sin\mathrm{i_O}\sin\Omega_{\mathrm{O}} & \sin\mathrm{i_O}\cos\Omega_{\mathrm{O}} & -\cos\mathrm{i_O} \\ -\cos\mathrm{u}\cos\Omega_{\mathrm{O}} + \sin\mathrm{u}\cos\mathrm{i_O}\sin\Omega_{\mathrm{O}} & -\cos\mathrm{u}\sin\Omega_{\mathrm{O}} - \sin\mathrm{u}\cos\mathrm{i_O}\cos\Omega_{\mathrm{O}} & -\sin\mathrm{u}\sin\mathrm{i_O} \end{bmatrix} \end{aligned} \tag{6}$$

where

$$u = \omega_O + \theta_O \tag{7}$$

Body. Body coordinate frame is defined by rotating orbital coordinate frame in the Z_O by the same amount as the satellite yaw angle, Ψ_B, then rotating in the new Y axis by the same amount as the satellite pitch angle, θ_B, and rotating in the new X-axis by the same amount as the satellite roll angle, φ_B. Orbital – Body transformation illustration can be seen in Figure 4. The transformation matrix from the orbital coordinate frame to the satellite coordinate frame, $\boldsymbol{R}_{\mathrm{O}}^{\mathrm{B}}$, can be formed as equation (8).

$$\begin{aligned}\boldsymbol{R}_{\mathrm{O}}^{\mathrm{B}} &= R_x(\varphi_B)R_y(\theta_B)R_z(\Psi_B) = \begin{bmatrix}1 & 0 & 0\\ 0 & \cos\varphi_B & \sin\varphi_B\\ 0 & -\sin\varphi_B & \cos\varphi_B\end{bmatrix}\begin{bmatrix}\cos\theta_B & 0 & -\sin\theta_B\\ 0 & 1 & 0\\ \sin\theta_B & 0 & \cos\theta_B\end{bmatrix}\begin{bmatrix}\cos\Psi_B & \sin\Psi_B & 0\\ -\sin\Psi_B & \cos\Psi_B & 0\\ 0 & 0 & 1\end{bmatrix}\\ &= \begin{bmatrix}\cos\theta_B\cos\Psi_B & \cos\theta_B\sin\Psi_B & -\sin\theta_B\\ \sin\varphi_B\sin\theta_B\cos\Psi_B - \cos\varphi_B\sin\Psi_B & \sin\varphi_B\sin\theta_B\sin\Psi_B + \cos\varphi_B\cos\Psi_B & \sin\varphi_B\cos\theta_B\\ \cos\varphi_B\sin\theta_B\cos\Psi_B + \sin\varphi_B\sin\Psi_B & \cos\varphi_B\sin\theta_B\sin\Psi_B - \sin\varphi_B\cos\Psi_B & \cos\varphi_B\cos\theta_B\end{bmatrix}\end{aligned} \tag{8}$$

Magnetometer. A magnetometer coordinate frame must be added since the coordinate frame does not coincide with the satellite coordinate frame in the LAPAN-A2 case. The frame, $\boldsymbol{R}_{\mathrm{mag}}^{\mathrm{B}}$, can be formed in equation (9).

$$\begin{aligned}\boldsymbol{R}_{\mathrm{mag}}^{\mathrm{B}} &= R_x(-90^0)R_y(0)R_z(90^0) = \begin{bmatrix}1 & 0 & 0\\ 0 & 0 & -1\\ 0 & 1 & 0\end{bmatrix}\begin{bmatrix}1 & 0 & 0\\ 0 & 1 & 0\\ 0 & 0 & 1\end{bmatrix}\begin{bmatrix}0 & 1 & 0\\ -1 & 0 & 0\\ 0 & 0 & 1\end{bmatrix}\\ &= \begin{bmatrix}0 & -1 & 0\\ 0 & 0 & 1\\ -1 & 0 & 0\end{bmatrix}\end{aligned} \tag{9}$$

4. NUMERICAL MODELLING

This section will explain numerical modelling which includes the orbit propagation model [16], the sun position model [17], the geomagnetic model [18], the TRIAD method [10], the kinematic method [19] and the EKF Method [20]. The illustration for numerical model can be seen in Fig. 6 – 8.

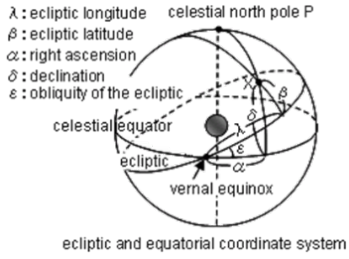

Fig. 6 Sun Position in Ecliptic and Equatorial Coordinate

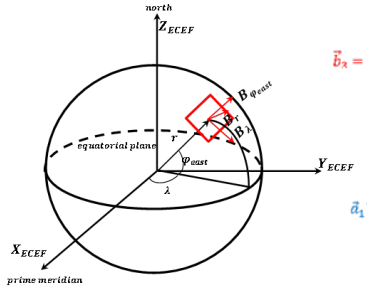

Fig. 7 Magnetic Field Generated by IGRF Model Illustration

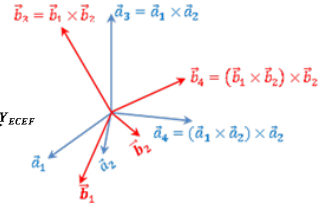

Fig. 8 TRIAD Method Illustration

Orbit Propagation Model. The NORAD general perturbation element sets are used to estimate the satellites' position and velocity. To achieve this, one must take control to implement a prediction technique that is appropriate for the method in which the elements were generated.

On all residing space objects, NORAD keeps general perturbation element sets (Two Line Elements, or TLEs). The periodic refinement of these element sets helps to maintain a fair level of prediction accuracy for all space objects. Users are then given access to these element

sets. The mean elements used in the NORAD element sets were removed in a specific way from periodic variations. These periodic changes must be recreated in the same method that NORAD removed them in order to produce accurate predictions. Therefore, even if a different model is more precise or even a numerical integrator, entering NORAD element sets into it will lead to subpar predictions. To maintain the highest level of prediction accuracy, one of the models mentioned in this report must be employed with the NORAD element sets.

In addition to producing predictions based on NORAD TLEs, the Special General Perturbation (SGP4) model also enables rapid calculations. Ken Cranford created the SGP4 model in 1970 [16]. This model was created by simplifying the more complex analytical theory of Lane and Cranford, which uses a power density function for its atmospheric model and Brouwer's solution for its gravitational model. The procedure to compute position and velocity state vectors for any desired time using SGP4 is well understood and detailed in Mahooti [16].

To apply the SGP4 method, the NORAD TLE from LAPAN A2 which is close to the observation time must be obtained and used as input plus the observation time which has been converted to Mean Julian Date (MJD) [16]. The output of this program is the position of the LAPAN A2 satellite in the ECI and ECEF coordinate frames.

Sun Position Model. The Sun's position in the sky is a function of both the time and the geographic location of observation on the Earth's surface. In relation to the fixed stars on the celestial sphere, the Sun appears to revolve along a circular path known as the ecliptic, as Earth orbits the Sun over the period of a year. Since the sun's position is desired in an inertial frame, the observer's geographic position can be neglected. It will be much easier to define the sun in ecliptic coordinates since ecliptic latitude will be zero and only define the sun's ecliptic longitude, λ_{sun}. Then, the sun's position in the ecliptic coordinate frame will be converted to the equatorial coordinate frame. ECI – ecliptic coordinate frame illustration can be seen in Figure 6. As can be seen in Fig.6, the obliquity of the ecliptic, ε_{ecl} need to described. This process is already done in [17] as a function of Julian Date, JD.

Start by calculating n_{day}, the number of days (positive or negative, including fractional days) since Greenwich noon, Terrestrial Time, on January 1, 2000 (J2000.0). If the Julian date for the desired time is known, then n_{day} can be calculated as equation (11).

$$n_{day} = \text{JD-2451545.0} \tag{10}$$

Then, the mean longitude of the Sun, L_{sun}, corrected for the aberration of light, can be calculated as equation (11).

$$L_{sun} = 280.4606184^0 + \frac{36000.77005361}{36525} n_{day} \text{ (degrees)} \tag{11}$$

Then, the mean anomaly of the Sun, g_{sun}, (Actually, of the Earth in its orbit around the Sun, but it is convenient to pretend the Sun orbits the Earth) can be calculated as equation (12).

$$g_{sun} = 357.5277233^0 + \frac{35999.05034}{36525} n_{day} \text{ (degrees)} \tag{12}$$

Finally, the ecliptic longitude of the Sun, λ_{sun}, is calculated as equation (13).

$$\lambda_{sun} = L_{sun} + 1.914666471 \sin g_{sun} + 0.918994643 \sin 2g_{sun} \tag{13}$$

Where the obliquity of the ecliptic, ε_{ecl}, can be approximated by equation (14).

$$\varepsilon_{ecl} = 23.43929^0 - \frac{46.8093}{3600} \frac{n_{day}}{36525} \text{ (degrees)} \tag{14}$$

Finally, the unit vector of sun position in the ECI coordinate, $\hat{\boldsymbol{x}}^{\mathrm{I}}_{\mathrm{sun}}$, can be approximated as equation (15):

$$\hat{\boldsymbol{x}}^{\mathrm{I}}_{\mathrm{sun}} = \begin{bmatrix} \cos\lambda_{\mathrm{sun}} \\ \cos\varepsilon_{\mathrm{ecl}} \sin\lambda_{\mathrm{sun}} \\ \sin\ \varepsilon_{\mathrm{ecl}} \sin\lambda_{\mathrm{sun}} \end{bmatrix}^{\mathrm{T}} \tag{15}$$

Geomagnetic Model. The most common geomagnetic model used is the International Geomagnetic Reference Field (IGRF). The IGRF a series of mathematical models describing the large-scale internal part of the Earth's magnetic field between epochs of 1900 A.D. and the present. The IGRF has been maintained and produced by an international team of scientists under the auspices of the International Association of Geomagnetism and Aeronomy (IAGA) since 1965 [18]. The IGRF model needs to be updated frequently in order to identify the ongoing temporal changes of the geomagnetic field produced in the outer core of the Earth. The IGRF model is revised at least once every 5 years and has now reached its 13th model. IGRF-12 was agreed upon in December 2014 by a task force of the IAGA Working Group V-MOD.

The IGRF is a series of mathematical models of the internal geomagnetic field $\vec{\boldsymbol{B}}(\mathrm{r},\ \lambda,\ \varphi_{\mathrm{east}},\ \mathrm{t})$ and its annual rate of change (secular variation). On and above the Earth's surface, the magnetic field $\vec{\boldsymbol{B}}$ is defined in terms of a magnetic scalar potential V by $\vec{\boldsymbol{B}} = -\nabla V$ and where in spherical polar co-ordinates V is approximated by the finite series in equation (15).

$$V(\mathrm{r},\ \lambda,\ \varphi_{\mathrm{east}},\ \mathrm{t}) = \mathrm{a}_{\mathrm{geomag}} \sum_{n=1}^{N} \sum_{m=1}^{n} \left(\frac{\mathrm{a}_{\mathrm{geomag}}}{\mathrm{r}}\right)^{n+1} [\mathrm{g}_{\mathrm{n}}^{\mathrm{m}}(\mathrm{t}) \cos(\mathrm{m}\varphi_{\mathrm{east}}) + \mathrm{h}_{\mathrm{n}}^{\mathrm{m}}(\mathrm{t}) \sin(\mathrm{m}\varphi_{\mathrm{east}})] \mathrm{P}_{\mathrm{n}}^{\mathrm{m}}(\cos\lambda) \tag{16}$$

Where r is radial distance from the center of the Earth (km), $\mathrm{a}_{\mathrm{geomag}}$ = 6371.2 km being the geomagnetic conventional Earth's mean reference spherical radius, λ is geocentric co-latitude (degree), φ_{east} is east longitude (degree), $\mathrm{P}_{\mathrm{n}}^{\mathrm{m}}$ *is* the Schmidt quasi-normalized associated Legendre functions of degree n and order m, and $\mathrm{g}_{\mathrm{n}}^{\mathrm{m}}$, $\mathrm{h}_{\mathrm{n}}^{\mathrm{m}}$ are The Gaussian coefficients as functions of time and are conventionally given in units of nanotesla (nT).

Usually, the change in the IGRF model refers to the change the Gaussian coefficient $\mathrm{g}_{\mathrm{n}}^{\mathrm{m}}$ and $\mathrm{h}_{\mathrm{n}}^{\mathrm{m}}$. The magnetic field obtained from IGRF model still in spherical coordinate $\vec{\boldsymbol{B}} = (\mathrm{B}_{\mathrm{r}}, \mathrm{B}_{\lambda}, \mathrm{B}_{\varphi_{\mathrm{east}}})$, meanwhile a magnetic field in the inertial frame is used for attitude estimation. Therefore, the result from IGRF needs to be transformed. The illustration of the magnetic field generated by the IGRF model can be seen in Figure 7. The magnetic field generated based on Figure 7 is known to be correlated with the NED coordinate frame. Then magnetic field in the NED coordinate frame can be formed by equation (17).

$$\hat{\boldsymbol{B}}_{\mathrm{NED}} = (\mathrm{B}_{\mathrm{north}}, \mathrm{B}_{\mathrm{east}}, \mathrm{B}_{\mathrm{down}}) = (-\mathrm{B}_{\lambda}, \mathrm{B}_{\varphi_{\mathrm{east}}}, -\mathrm{B}_{\mathrm{r}}) \tag{17}$$

Finally, unit vector of the magnetic field in the ECI coordinate, $\hat{\boldsymbol{x}}^{\mathrm{I}}_{\mathrm{mag}}$,can be formed by transforming the magnetic field in the NED coordinate frame to the ECEF coordinate frame, then, from the ECEF coordinate frame to the ECI coordinate frame. The transformation can be described by equation (18).

$$\hat{\boldsymbol{x}}^{\mathrm{I}}_{\mathrm{mag}} = \boldsymbol{R}^{\mathrm{I}}_{\mathrm{E}} \boldsymbol{R}^{\mathrm{E}}_{\mathrm{NED}} \hat{\boldsymbol{B}}_{\mathrm{NED}} \tag{18}$$

TRIAD Method. Three Axes Attitude Determination, also known as TRIAD, is a deterministic attitude estimation method. The TRIAD method works by calculating the rotation matrix from a set (minimal two) of vectors in inertial frame which is described in this research as an enviroment model to a set of vectors in reference frame which is described in this research as sensor measurements [10].

Let consider environmental model vectors $(\vec{\boldsymbol{a}}_1, \vec{\boldsymbol{a}}_2)$ and sensor measurement vectors $(\vec{\boldsymbol{b}}_1, \vec{\boldsymbol{b}}_2)$. Then, for coherent solution, rotation matrix $\boldsymbol{A}$ must satisfy two solutions $\vec{\boldsymbol{b}}_1 = \boldsymbol{A}\vec{\boldsymbol{a}}_1$ and $\vec{\boldsymbol{b}}_2 = \boldsymbol{A}\vec{\boldsymbol{a}}_2$. Since the problem consists of two solutions, and the rotation matrix is 3 by 3 in size, the third equation must be introduced. The third equation can be formed by using the orthogonal vector of the same reference, $\vec{\boldsymbol{a}}_3 \perp \vec{\boldsymbol{a}}_2$ and $\vec{\boldsymbol{a}}_3 \perp \vec{\boldsymbol{a}}_1$ also $\vec{\boldsymbol{b}}_3 \perp \vec{\boldsymbol{b}}_2$ and $\vec{\boldsymbol{b}}_3 \perp \vec{\boldsymbol{b}}_1$. The illustration for the TRIAD method can be seen in Figure 8. Figure 8 shows coherent solution rotation matrix $\boldsymbol{A}$ obtained as a rotation matrix from one coordinat frame into another coordinat frame. For a better solution, it is suggested that the vectors from one reference must be orthonormal. Then here below is the procedure for obtaining the rotation matrix $\boldsymbol{A}$.

Consider the vectors of environmental models $(\vec{\boldsymbol{a}}_1, \vec{\boldsymbol{a}}_2)$ and sensor measurement vectors $(\vec{\boldsymbol{b}}_1, \vec{\boldsymbol{b}}_2)$. For the orthonormal vector, $\boldsymbol{a}_3$ and $\boldsymbol{b}_3$ must be formed by equation (19).

$$\vec{\boldsymbol{a}}_3 = \frac{\vec{\boldsymbol{a}}_1 \times \vec{\boldsymbol{a}}_2}{\|\vec{\boldsymbol{a}}_1 \times \vec{\boldsymbol{a}}_2\|} \; and \; \vec{\boldsymbol{b}}_3 = \frac{\vec{\boldsymbol{b}}_1 \times \vec{\boldsymbol{b}}_2}{\|\vec{\boldsymbol{b}}_1 \times \vec{\boldsymbol{b}}_2\|} \tag{19}$$

Then for the orthonormal third axis, it can be formed as equation (20).

$$\vec{\boldsymbol{a}}_4 = \frac{(\vec{\boldsymbol{a}}_1 \times \vec{\boldsymbol{a}}_2) \times \vec{\boldsymbol{a}}_1}{\|(\vec{\boldsymbol{a}}_1 \times \vec{\boldsymbol{a}}_2) \times \vec{\boldsymbol{a}}_1\|} \; and \; \vec{\boldsymbol{b}}_4 = \frac{(\vec{\boldsymbol{b}}_1 \times \vec{\boldsymbol{b}}_2) \times \vec{\boldsymbol{b}}_1}{\|(\vec{\boldsymbol{b}}_1 \times \vec{\boldsymbol{b}}_2) \times \vec{\boldsymbol{b}}_1\|} \tag{20}$$

A coordinate transformation matrix equation can be formed as equation (21).

$$[\vec{\boldsymbol{a}}_1^{\mathrm{T}} \quad \vec{\boldsymbol{a}}_4^{\mathrm{T}} \quad \vec{\boldsymbol{a}}_3^{\mathrm{T}}] = \boldsymbol{A}[\vec{\boldsymbol{b}}_1^{\mathrm{T}} \quad \vec{\boldsymbol{b}}_4^{\mathrm{T}} \quad \vec{\boldsymbol{b}}_3^{\mathrm{T}}] \tag{21}$$

Since the vector is orthonormal, the rotation matrix $\boldsymbol{A}$ can be formed by equation (22).

$$\boldsymbol{A} = [\vec{\boldsymbol{a}}_1^{\mathrm{T}} \quad \vec{\boldsymbol{a}}_4^{\mathrm{T}} \quad \vec{\boldsymbol{a}}_3^{\mathrm{T}}][\vec{\boldsymbol{b}}_1^{\mathrm{T}} \quad \vec{\boldsymbol{b}}_4^{\mathrm{T}} \quad \vec{\boldsymbol{b}}_3^{\mathrm{T}}]^{\mathrm{T}} \tag{22}$$

In this research, $\vec{\boldsymbol{a}}_1$ is the sun position in ECI coordinate, $\vec{\boldsymbol{x}}_{\mathrm{sun}}^{\mathrm{I}}$, $\vec{\boldsymbol{a}}_2$ is the magnetic field in ECI coordinate, $\vec{\boldsymbol{x}}_{\mathrm{mag}}^{\mathrm{I}}$, $\vec{\boldsymbol{b}}_1$ is the sun position in body coordinate, $\vec{\boldsymbol{x}}_{\mathrm{sun}}^{\mathrm{B}}$, $\vec{\boldsymbol{b}}_2$ is the magnetic field in body coordinate, $\vec{\boldsymbol{x}}_{\mathrm{mag}}^{\mathrm{B}}$, and $\boldsymbol{A}$ is the rotation matrix between inertial and body coordinate frame, $\boldsymbol{R}_{\mathrm{I}}^{\mathrm{B}}$. However, the obtained rotation matrix doesn't represent the attitude of satellite. The attitude of satellite is defined by the rotation between orbital coordinate and body coordinate system, $\boldsymbol{R}_{\mathrm{O}}^{\mathrm{B}}$, must be found. The body coordinate system can be calculated using equation (23) and (24).

$$\boldsymbol{R}_{\mathrm{I}}^{\mathrm{B}} = \boldsymbol{R}_{\mathrm{O}}^{\mathrm{B}} \boldsymbol{R}_{I}^{O} \tag{23}$$

$$\boldsymbol{R}_{O}^{\mathrm{B}} = \boldsymbol{R}_{I}^{\mathrm{B}} \boldsymbol{R}_{I}^{O^{-1}} \tag{24}$$

where rotation matrix between from the ECI coordinate frame to the orbital coordinate frame, $\boldsymbol{R}_{\mathrm{I}}^{\mathrm{O}}$, can be obtained by equation (8). The matrix elements from equation (8) obtained by position and velocity obtained from SGP4 and transformed into orbital elements. The rotation between orbital coordinate and body coordinate system, $\boldsymbol{R}_{\mathrm{O}}^{\mathrm{B}}$, however, are still not adequately describe the attitude of the satellite. The proper representation of a satellite attitude is the Euler angle. So, the rotation matrix will be transformed into a quaternion for stability output, then transformed into an Euler angle.

The procedure described by Blanco [21] is from equation (25) to equation (31). Consider matrix element from the obtained matrix, $\boldsymbol{R}_{\mathrm{O}}^{\mathrm{B}}$.

$$\boldsymbol{R}_{\mathrm{O}}^{\mathrm{B}} = \begin{bmatrix} \mathrm{R}_{11} & \mathrm{R}_{12} & \mathrm{R}_{13} \\ \mathrm{R}_{21} & \mathrm{R}_{22} & \mathrm{R}_{23} \\ \mathrm{R}_{31} & \mathrm{R}_{32} & \mathrm{R}_{33} \end{bmatrix} \tag{25}$$

Create an intermediate variable $\begin{bmatrix} t_s & t_x & t_y & t_z \end{bmatrix}$

$$\begin{bmatrix} t_s & t_x & t_y & t_z \end{bmatrix} = \left[\sqrt{\frac{1}{4}(1 + \mathrm{R}_{11} + \mathrm{R}_{22} + \mathrm{R}_{33})} \sqrt{\frac{1}{4}(1 + \mathrm{R}_{11} - \mathrm{R}_{22} - \mathrm{R}_{33})} \sqrt{\frac{1}{4}(1 - \mathrm{R}_{11} + \mathrm{R}_{22} - \mathrm{R}_{33})} \sqrt{\frac{1}{4}(1 - \mathrm{R}_{11} - \mathrm{R}_{22} + \mathrm{R}_{33})} \right] \tag{26}$$

Consider quaternion vector element $\boldsymbol{q} = \begin{bmatrix} \mathrm{q_s}, \mathrm{q_x}, \mathrm{q_y}, \mathrm{q_z} \end{bmatrix}^T$. The quaternion value will be obtained by using if max function in equation (27).

If max	$\boldsymbol{q} = \begin{bmatrix} \mathrm{q_s}, \mathrm{q_x}, \mathrm{q_y}, \mathrm{q_z} \end{bmatrix}$	If max	$\boldsymbol{q} = \begin{bmatrix} \mathrm{q_s}, \mathrm{q_x}, \mathrm{q_y}, \mathrm{q_z} \end{bmatrix}$
t_s	$\left[t_s, \frac{\mathrm{R}_{32} - \mathrm{R}_{23}}{4t_s}, \frac{\mathrm{R}_{13} - \mathrm{R}_{31}}{4t_s}, \frac{\mathrm{R}_{21} - \mathrm{R}_{12}}{4t_s} \right]$	t_y	$\left[\frac{\mathrm{R}_{13} - \mathrm{R}_{31}}{4t_y}, \frac{\mathrm{R}_{21} + \mathrm{R}_{12}}{4t_y}, t_y, \frac{\mathrm{R}_{32} + \mathrm{R}_{23}}{4t_y} \right]$
t_x	$\left[\frac{\mathrm{R}_{32} - \mathrm{R}_{23}}{4t_x}, t_x, \frac{\mathrm{R}_{21} + \mathrm{R}_{12}}{4t_x}, \frac{\mathrm{R}_{13} + \mathrm{R}_{31}}{4t_x} \right]$	t_z	$\left[\frac{\mathrm{R}_{21} - \mathrm{R}_{12}}{4t_z}, \frac{\mathrm{R}_{13} + \mathrm{R}_{31}}{4t_z}, \frac{\mathrm{R}_{32} + \mathrm{R}_{23}}{4t_z}, t_z \right]$

(27)

Then the quaternion vector obtained in the equation (27) is converted into an euler angle. Consider a quaternion difference, Δ.

$$\Delta = \mathrm{q_s q_y} - \mathrm{q_x q_z} \tag{28}$$

If $|\Delta| < 0.5$ $$\Psi_{\mathrm{B}} = \tan^{-1}\left(2\frac{\mathrm{q_s q_z} + \mathrm{q_x q_y}}{1 - 2(\mathrm{q_y^2} + \mathrm{q_z^2})}\right), \theta_{\mathrm{B}} = \sin^{-1}(2\Delta), \text{and } \varphi_{\mathrm{B}} = \tan^{-1}\left(2\frac{\mathrm{q_s q_x} + \mathrm{q_y q_z}}{1 - 2(\mathrm{q_x^2} + \mathrm{q_y^2})}\right) \tag{29}$$

If $\Delta = -0.5$ $$\Psi_{\mathrm{B}} = 2\tan^{-1}\left(\frac{\mathrm{q_x}}{\mathrm{q_s}}\right), \theta_{\mathrm{B}} = -\frac{\pi}{2}, \text{and } \varphi_{\mathrm{B}} = 0 \tag{30}$$

If $\Delta = 0.5$ $$\Psi_{\mathrm{B}} = -2\tan^{-1}\left(\frac{\mathrm{q_x}}{\mathrm{q_s}}\right), \theta_{\mathrm{B}} = \frac{\pi}{2}, \text{and } \varphi_{\mathrm{B}} = 0 \tag{31}$$

Kinematic Method. Kinematic method is used to examine rotations that evolve over time. With the attitude kinematics, they provide a relation between the time derivative of attitude representation and angular velocity. The complete process is explained in Tewari [19] with the time derivative of quaternion in body coordinate respect to the inertial frame, $\dot{\boldsymbol{q}}_{\mathrm{I}}^{\mathrm{B}}$, shown in equation (32).

$$\dot{\boldsymbol{q}}_{\mathrm{I}}^{\mathrm{B}} = \frac{1}{2}\Omega\left(\boldsymbol{\omega}_{\mathrm{I}}^{\mathrm{B}}\right)\boldsymbol{q}_{\mathrm{I}}^{\mathrm{B}} \tag{32}$$

where $\boldsymbol{q}_{\mathrm{I}}^{\mathrm{B}}$ is quaternion representative of the body frame with respect to the inertial frame, $\boldsymbol{q}_{\mathrm{I}}^{\mathrm{B}} = \begin{bmatrix} \mathrm{q_s} & \mathrm{q_x} & \mathrm{q_y} & \mathrm{q_z} \end{bmatrix}^T$, ω_I^B is the vector angular velocity of the body frame with respect to the inertial frame obtained from gyroscope measurement, $\boldsymbol{\omega}_{\mathrm{I}}^{\mathrm{B}} = [\omega_{\mathrm{x}} \quad \omega_{\mathrm{y}} \quad \omega_{\mathrm{z}}]^T$, and $\Omega(\cdot)$ is a skew – symmetric matrix of angular velocity as can be described in equation (33).

$$\Omega = \begin{bmatrix} 0 & -\omega_x & -\omega_y & -\omega_z \\ \omega_{\mathrm{x}} & 0 & \omega_{\mathrm{z}} & -\omega_{\mathrm{y}} \\ \omega_{\mathrm{y}} & -\omega_{\mathrm{z}} & 0 & \omega_{\mathrm{x}} \\ \omega_{\mathrm{z}} & \omega_{\mathrm{y}} & -\omega_{\mathrm{x}} & 0 \end{bmatrix} \tag{33}$$

Attitude kinematics in this research will be used as a prediction state in the EKF method since neither desired attitude input nor control system is given. A prediction state will be

obtained by integrating the quaternion derivative in equation (32) This method is very dependent on the initial conditions.

Extended Kalman Filter (EKF). The methods explained in previous subchapter have significant issues. First, gyroscope measurement errors in attitude kinematics are integrated. During long time periods of operation, error integration in gyroscope measurement causes divergence. Second, the TRIAD method as a vector method produces measurements that have strong oscillations depending on how severe the disturbances are in the sun sensor and magnetometer. The stochastic filtering method can perform the fusion of data originated from different methods. By fusing the two methods explained, the TRIAD method can prevent the divergence of gyroscope integration, while the attitude kinematic can smooth the TRIAD oscillations. The Kalman Filter (KF) is the most widely used stochastic filtering technique. The Kalman filter method has two phases: The prediction phase generates the state vector one step ahead. While the correction phase corrects the prediction by using the most current reading from another sensor, The prediction phase in this research uses attitude kinematics, while the correction phase uses the TRIAD method. To solve the non-linear system, the Extended Kalman filter (EKF) is used, which performs non-linear approximations. The procedure of EKF was done by Jategaonkar [20] in equation (34) to equation (42). Consider the nonlinear system equation in equation (34), which predicts the following state:

$$\dot{x} = f(x,u,t) + G(x,t)w(t) \tag{34}$$

Where x is the state of the system (quaternion), f is the state function, u is the entry variable (angular velocity),and w is the noise of the gyroscope or process noise that has a variance matrix, Q_{KF}. With measurement state equation is formed in equation (35).

$$z(\mathrm{t}) = h(x) + v(\mathrm{t}) \tag{35}$$

Where z is the measurement state, h is the measurement function, and v is the noise of the measurement vector that has a variance matrix, R_{KF}. The error covariance equation(36).

$$\dot{\boldsymbol{P}} = \boldsymbol{F}_k P(t) + P(t)\boldsymbol{F}_k^{\mathrm{T}} + \boldsymbol{Q}_k'' \tag{36}$$

where $\boldsymbol{F}_k = \partial f/\partial x\,|_{x=\hat{x}_k^+}$, $\hat{x}_k^+$, and $\boldsymbol{Q}_k''$ is defined in equation (37).

$$\boldsymbol{Q}_k'' = G(\hat{x}_k^+, t_k) Q_{KF}(t_k) G^{\mathrm{T}}(\hat{x}_k^+, \mathrm{t_k}) \tag{37}$$

Then the EKF procedure can be summarized as: First, the prediction phase: Calculate the prediction state, $\hat{x}_{k+1}^-$, at the time of the next iteration, t_{k+1} in equation (38).

$$\hat{\boldsymbol{x}}_{k+1}^- = \hat{\boldsymbol{x}}_k^+ + \int_{t_k}^{t_{k+1}} f(x,u,t)\mathrm{d}t \tag{38}$$

Then calculate the prediction covariance, P_{k+1}^- in equation (39).

$$\boldsymbol{P}_{k+1}^- = \boldsymbol{P}_k^+ + \int_{t_k}^{t_{k+1}} \dot{P}(t)\mathrm{d}t \tag{39}$$

Second, the kalman gain $\bar{\boldsymbol{K}}_k$ obtained in equation (40)

$$\bar{\boldsymbol{K}}_k = \boldsymbol{P}_{k+1}^- \boldsymbol{H}_k^{\mathrm{T}} \left(\boldsymbol{H}_k \boldsymbol{P}_{k+1}^- \boldsymbol{H}_k^{\mathrm{T}} + \boldsymbol{R}_{KF_k}\right)^{-1} \tag{40}$$

where $H_k = \partial h/\partial x\,|_{x=\hat{x}_{k+1}^-}$ is the linearization of the measurement function. And finally, the correction phase. Calculate the correction state, $\hat{x}_{k+1}^+$ in equation (41).

$$\hat{\boldsymbol{x}}_{k+1}^+ = \hat{\boldsymbol{x}}_{k+1}^- + \bar{\boldsymbol{K}}_{\boldsymbol{k}}[z_k - h(\hat{x}_{k+1}^-)] \tag{41}$$

And the final step is to correct the error covariance, $\boldsymbol{P}_{k+1}^{+}$ in equation (42).

$$\boldsymbol{P}_{k+1}^{+} = \boldsymbol{P}_{k+1}^{-} - \bar{\boldsymbol{K}}_k \boldsymbol{H}_k \boldsymbol{P}_{k+1}^{-} \tag{42}$$

Many real-world problems are based on a physical system that is continuous in time with discrete time measurements. Then, discrete form of the prediction state in equation (43).

$$\hat{\boldsymbol{x}}_{k+1}^{-} = \boldsymbol{\Phi}_k \hat{\boldsymbol{x}}_k^{+} \tag{43}$$

where Φ_{k} is the discrete form of matrix F_k and recall equation (32). $\boldsymbol{\Phi}_k$ in equation (44).

$$\boldsymbol{\Phi}_k = e^{\frac{1}{2}\Omega(\omega_k)(t_{k+1}-t_k)} \tag{44}$$

And prediction covariance will be obtained in equation (45).

$$\boldsymbol{P}_{k+1}^{-} = \boldsymbol{\Phi}_k \boldsymbol{P}_k^{+} \boldsymbol{\Phi}_k^{\mathrm{T}} + \boldsymbol{\Gamma}_k Q_{KF}(t_k) {\boldsymbol{\Gamma}_k}^{\mathrm{T}} \tag{45}$$

where Γ_k is the discrete form of matrix $\boldsymbol{G}_k$ and described in equation (46).

$$\boldsymbol{\Gamma}_k = \boldsymbol{\Phi}_k (t_{k+1} - t_k) \tag{46}$$

For kalman gain and correction phase, the equation is the same as Eq. 3.47 – 3.49. Then, in this research, the innovation state $[z_k - h(\hat{x}_{k+1}^{-})]$ will be described in equation (47).

$$[z_k - h(\hat{x}_{k+1}^{-})] = y^{\mathrm{B}} - R_{\mathrm{I}}^{\mathrm{B}}(q) y^{I} = \begin{bmatrix} \mathrm{y_x^B} \\ \mathrm{y_y^B} \\ \mathrm{y_z^B} \end{bmatrix} - \begin{bmatrix} 2(\mathrm{q_x^2 + q_s^2}) - 1 & 2(\mathrm{q_x q_y + q_z q_s}) & 2(\mathrm{q_x q_z - q_y q_s}) \\ 2(\mathrm{q_x q_y - q_z q_s}) & 2(\mathrm{q_y^2 + q_s^2}) - 1 & 2(\mathrm{q_y q_z + q_x q_s}) \\ 2(\mathrm{q_x q_z + q_y q_s}) & 2(\mathrm{q_y q_z + q_x q_s}) & 2(\mathrm{q_z^2 + q_s^2}) - 1 \end{bmatrix} \begin{bmatrix} \mathrm{y_x^I} \\ \mathrm{y_y^I} \\ \mathrm{y_z^I} \end{bmatrix} \tag{47}$$

where $\begin{bmatrix} \mathrm{y_x^B} & \mathrm{y_y^B} & \mathrm{y_z^B} \end{bmatrix}^{\mathrm{T}}$ is the sensor measurement vector, $\begin{bmatrix} \mathrm{y_x^I} & \mathrm{y_y^I} & \mathrm{y_z^I} \end{bmatrix}^{\mathrm{T}}$ is the environmental model vector, and $R_{\mathrm{I}}^{\mathrm{B}}(q)$ is the transformation coordinate from the inertial frame to the body frame in form of a quaternion. The linearization of the output function, $\boldsymbol{H}_{\mathrm{k}}$, in equation (48).

$$\boldsymbol{H}_{\mathrm{k}} = \frac{\partial h(q)}{\partial q} = \begin{bmatrix} 4\mathrm{y_x^I q_s} + 2\mathrm{y_y^I q_z} - 2\mathrm{y_z^I q_y} & 4\mathrm{y_x^I q_x} + 2\mathrm{y_y^I q_y} + 2\mathrm{y_z^I q_z} & 2\mathrm{y_y^I q_x} - 2\mathrm{y_z^I q_s} & 2\mathrm{y_z^I q_x} + 2\mathrm{y_y^I q_s} \\ -2\mathrm{y_x^I q_z} + 4\mathrm{y_y^I q_s} + 2\mathrm{y_z^I q_x} & 2\mathrm{y_x^I q_y} + 2\mathrm{y_z^I q_s} & 2\mathrm{y_x^I q_x} + 4\mathrm{y_y^I q_y} + 2\mathrm{y_z^I q_z} & 2\mathrm{y_z^I q_y} - 2\mathrm{y_x^I q_s} \\ 2\mathrm{y_x^I q_y} - 2\mathrm{y_y^I q_x} + 4\mathrm{y_z^I q_s} & 2\mathrm{y_x^I q_z} - 2\mathrm{y_y^I q_s} & 2\mathrm{y_y^I q_z} + 2\mathrm{y_x^I q_s} & 2\mathrm{y_x^I q_x} + 2\mathrm{y_y^I q_y} + 4\mathrm{y_z^I q_z} \end{bmatrix} \tag{48}$$

5. RESULTS AND CONCLUSIONS

The results are generated by running the simulation model in the MATLAB programming code. Simulations were done in 4 different dates for testing the program reliability. For each case, there are several conditions to be met which can be seen in Table 2.

Table 2. Simulation Conditions for Cases

Variable/ Date (Cases)	**09/01/2017**	**31/03/2017**	**12/06/2017**	**04/09/2017**
mass, $\mathrm{m_B}(kg)$	74			
Simulation Epoch (in UTC)	04:05:29.0	06:59:21.5	05:06:53.0	03:55:37.0
Time Step, Δt(second)	0.5			
Simulation Time (Second)	607.0	622.0	752.0	564.5
Semi major axis, $\mathrm{a}(km)$	7018.51	7018.48	7018.44	7018.41
Eccentricity, $\mathrm{e}(-)$	0.0013	0.0013	0.0013	0.0014
Inclination, $\mathrm{i_O}(-)$	6.0	6.0	6.0	6.0
Right Ascension of Ascending Node, $\Omega_O(°)$	286.55	68.28	268.68	29.59
Argument of Perigee, $\omega_{\mathrm{O}}(°)$	156.66	220.22	174.05	282.97

Sensor Measurement Output. In this subchapter, sensor output obtained from the sun sensor and magnetometer has already changed into a unit vector. The angular rate measurement is in deg/s. The outputs can be seen in Figure 9 and Figure 10.

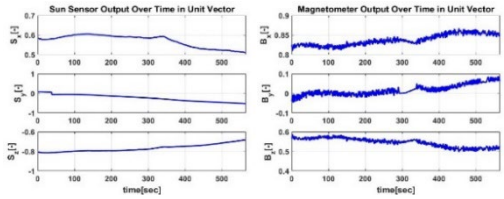

Fig. 9 Example of Sensor Output Over Time in Unit Vector from Sun Sensor (Left) and Magnetometer (Right) at 04 – 09 – 2017 Case

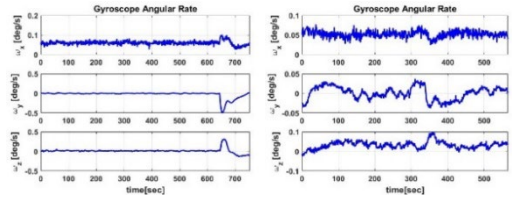

Fig. 10 Example of Angular Rate Measurement from Gyroscope Output at 12/06/17 (Left) and 04/09/17 (Right) Case

TRIAD Result. The TRIAD method is used to generate attitude by transforming equation (19) to equation (22) and equation (23) to equation (31). The result from TRIAD will be compared to the star sensor result and can be seen in Figure 11.

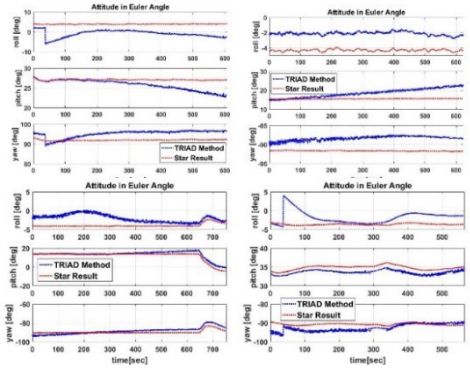

Fig. 11 TRIAD Result and Comparison with Star Sensor Euler Angle at 09/01/17 (Top Left), 31/03/17 (Top Right), 12/06/17 (Bottom Left), and 04/09/17 (Bottom Right) Case

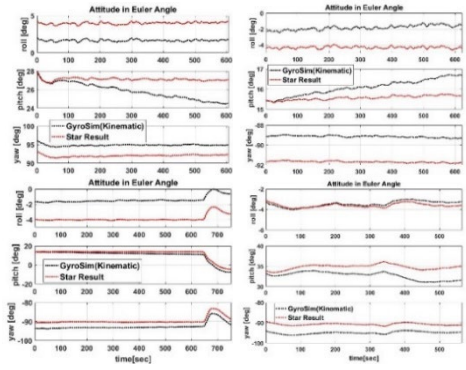

Fig. 12 Kinematic Result and Comparison at Star Sensor Euler Angle with 09/01/17 (Top Left), 31/03/17 (Top Right), 12/06/17 (Bottom Left), and 04/09/17 (Bottom Right) Case

Kinematic Result. After the TRIAD result has been obtained, the result at t=0 s can be used as an initial condition for the kinematic method. Then, the result for the next time step can be obtained by using the integration of equation (32) and the transformation from equation (23) to equation (31). The kinematic method result can be seen in Figure 12.

Kalman Filter Result. After obtaining results from TRIAD and the kinematic method, KF can be done by equation (38) to (48) with kinematic as the prediction state and TRIAD as the observation state. For measurement noise covariance, R_{KF} is assumed to be the same and also varies with constant process noise covariance, Q_{KF}. Results from the Kalman Filter can be seen from Figure 13 to Figure 15.

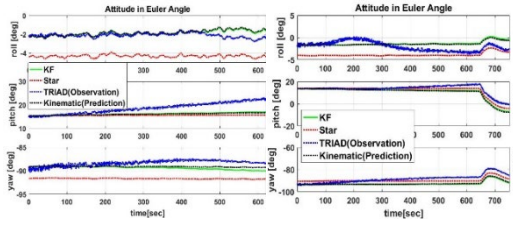

Fig. 13 Kalman Filter Result and Comparison with Star Sensor Euler Angle at 31/03/17 (Left), and 12/06/17 (Right) with $\mathrm{Q_{KF}} = 1 \times 10^{-9}, \mathrm{R_{KF}} = 1 \times 10^{-2}$ ($\mathrm{R_{KF}}/\mathrm{Q_{KF}} = 10^{7}$)

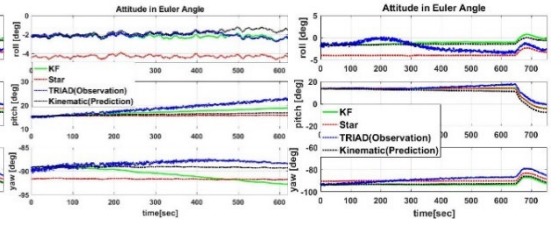

Fig. 14 Kalman Filter Result and Comparison with Star Sensor Euler Angle at 31/03/17 (Left), and 12/06/17 (Right) with $\mathrm{Q_{KF}} = 1 \times 10^{-9}, \mathrm{R_{KF}} = 1 \times 10^{-3}$ ($\mathrm{R_{KF}}/\mathrm{Q_{KF}} = 10^{6}$)

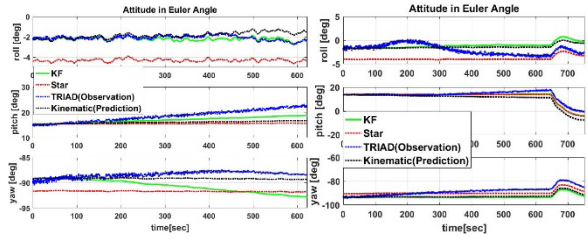

Fig. 15 Kalman Filter Result and Comparison with Star Sensor Euler Angle at 31/03/17 (Left), and 12/06/17 (Right) with $Q_{\mathrm{KF}} = 1 \times 10^{-9}$, $R_{\mathrm{KF}} = 1 \times 10^{-3}$ ($R_{\mathrm{KF}}/Q_{\mathrm{KF}} = 10^{6}$)

Figure 13 and 14 show Kalman Filter result with TRIAD as initial condition. Figure 13 with $R_{KF}/Q_{KF} = 10^{7}$ still adjacent to the prediction state. While in the Figure 14 with the lowered value of coefficient $\mathrm{R_{KF}/Q_{KF}} = 10^{6}$. Observational state starts to influence and gives results close to the star sensor results as the ideal value. The results of the Kalman filter as a whole in LAPAN A2 provide an ideal value for this coefficient value. However, an additional with the Kalman filter method will be carried out with the initial conditions being equal to the output of the star sensor as shown in Figure 15. Figure 15 shows that the results of the Kalman Filter are adjacent to the star sensor results and gives the best results at coefficient value, $\mathrm{R_{KF}/Q_{KF}} = 10^{7}$. However, the results are still deviated due to the divergent behaviour of the kinematic method and the coefficient values that give a tendency to the kinematic method.

The quantity evaluation of the methods used will be calculated using the Mean Absolute Error (MAE) based on [4,5,8,9]. The absolute error, $|e|$, is the discrepancy between the difference between calculated value (x_{calc}) and the actual/ideal value of a quantity (x_{ideal}): $|e| = |x_{calc} - x_{ideal}|$. The mean absolute of given state x is: $\mathrm{MAE} = 1/N \times \sum_i^N |x_{calc_i} - x_{ideal_i}|$. Table 3 summarize the MAE of cases evaluated with four days experiment that will be averaged within the same configuration.

The table also presents the result from previous research of LAPAN A2 [11] and the best result of previous research on Kalman Filter Method [3, 4, 5, 8, 9].

Table 3. Mean Absolute Error Comparison Between Methods

Method	**Variable**			
	$\mathbf{Q_{KF}}$	$\mathbf{R_{KF}}$	**R/Q**	**mean $\|e\|[deg]$**
LAPAN A2 Previous Research (TRIAD) [11]				3.50
TRIAD				2.42
Kinematic				2.14
Extended Kalman Filter (EKF)	$1 * 10^{-9}$	$1 * 10^{-2}$	$1 * 10^{7}$	2.12
	$1 * 10^{-9}$	$1 * 10^{-3}$	$1 * 10^{6}$	2.03
	$1 * 10^{-9}$	$1 * 10^{-6}$	$1 * 10^{3}$	3.01
	$1 * 10^{-6}$	$1 * 10^{-6}$	1	3.77
	$1 * 10^{-6}$	$1 * 10^{-9}$	$1 * 10^{-3}$	3.64
KF with Initial Star Result	$1 * 10^{-9}$	$1 * 10^{-2}$	$1 * 10^{7}$	0.19
Best KF result in another research [9]				0.12

Conclusions. The process of estimating attitudes from the output of sensors has been successfully carried out with various methods. The output of the sun sensor and magnetometer has been successfully transformed into an attitude by changing and converting the transformation matrix obtained from the TRIAD method between the sensor output and the environmental model. While the gyroscope output is used in the kinematic method with the initial conditions of the TRIAD method. The outputs of these three sensors are fused in the Extended Kalman Filter (EKF) method with various values of R/Q ratio. The best output of

the methods used is the EKF method with an R/Q ratio of 10^6 (MAE = 2.03 degree). The research also carried out EKF simulation with the initial conditions of the star sensor and obtained results close to the best results from the references used (MAE = 0.19 degree). Therefore, it can be concluded that selecting the right initial conditions can improve the performance of the estimation method. This also means that the bounded error that occurs in the TRIAD method for the initial conditions is quite large. Thus, it is necessary to improve deterministic estimation methods and environmental modeling for the output of sun sensors and magnetometers, and select satellite cases with more qualified sensor specifications in future research.

REFERENCES

[1] S. Hardhienata, R. H. Triharjanto, M. Mukhayadi, *LAPAN-A2: Indonesian Near-Equatorial Surveillance Satellite*, APRSAF-18 (Asia-Pacific Regional Space Agency Forum) Singapore, December 6-9, 2011.

[2] P. C. Agrawal, AstroSat: From Inception to Realization and Launch, *Journal of Astrophysics and Astronomy*, **38**(2), 1 – 8, 2011.

[3] T. Bak, *Spacecraft Attitude Determination: A Magnetometer Approach*, Ph.D. Thesis, Aalborg Universitetsforlag, Denmark, 1999.

[4] Y. Mimasu, J. C. Van der Ha, and T. Narumi, Attitude Determination by Magnetometer and Gyros during Eclipse, *AIAA/AAS Astrodynamics Specialist Conference and Exhibit*, Japan, 2008.

[5] A. Walker, and M. Kumar, CubeSat Attitude Determination Using Low-Cost Sensors and Magnetic Field Time Derivative, *55th AIAA Aerospace Sciences Meeting*, (January), 1–24, 6, Ohio, USA, 2017.

[6] G. Wahba, A Least Squares Estimate of Satellite Attitude, *SIAM Review* **7**(3), 409, 1965.

[7] S. Marques, R. Clements, and P. Lima, Comparison of small satellite attitude determination methods, *AIAA Guidance, Navigation, and Control Conference*, Denver, 2000.

[8] K. Maier, A. Luis, and F. Coelho, Attitude Determination for A Brazilian Cubesat Mission Using the Kalman Filter, *24th ABCM International Congress of Mechanical Engineering*, Brazil, 2017.

[9] M. Ovchinnikov, and D. Ivanov, Approach to study satellite attitude determination algorithms, *Acta Astronautica*, **98**(1), 133–137, Russia, 2014.

[10] G. M. Lerner, *Spacecraft Attitude Determination and Control, Chap. Three-Axis Attitude Determination*, pp. 420–428, Reidel, Dordrecht, The Netherlands, 1978.

[11] S. Utama, and P. R. Hakim, *Sun Sensor and Magnetometer as Attitude Determination Sensors for Low Inclination Satellite Lapan A-2, LAPAN*, Indonesia, 2018.

[12] J. R. Wertz, *Spacecraft Attitude Determination and Control*, Kluwer Academic Publishers, 1978.

[13] F. L. Markley, Attitude Determination Using Vector Observations and the Singular Value Decomposition, *Journal of the Astronautical Sciences* **3**6(3), 245–258, 1988.

[14] D. A. Vallado, *Fundamental of Astrodynamics and Applications*, 4th ed. Colorado, USA. The Space Tecnology Library, 2013.

[15] M. A. Saifudin and M. Mukhayadi, *Sistem Attitude Determination and Control (ADCS) Satelit LAPAN-A2/Orari*, Media Dirgantara, 39 – 46, Indonesia, 2015.

[16] M. Mahooti, SGP4 (https://www.mathworks.com/ matlabcentral/ fileexchange/62013-sgp4), *MATLAB Central File Exchange*, Retrieved July 28, 2022.

[17] * * * U.S. Naval Observatory, U. K. Hydrographic Office, H. M. Nautical Almanac Office, *The Astronomical Almanac for the Year 2010*, U. S. Govt. Printing Office, p. C5. ISBN 978-0-7077-4082-9, USA, 2008.

[18] Thébault et al., *Earth, Planets and Space. International Geomagnetic Reference Field: The 12th generation*, Springer, France, 2015.

[19] A. Tewari, *Atmospheric and Space Flight Dynamics: Modeling and simulation with MATLAB and Simulink*, Birkhauser Boston, 1st edition, India, 2007.

[20] R. V. Jategaonkar, Flight Vehicle System Identification – A Time Domain Methodology, *AIAA Progress in Astronautics and Aeronautics*, AIAA, New York, USA, 2006.

[21] J. Blanco, *A tutorial on SE (3) transformation parameterizations and on-manifold optimization*, University of Malaga, Tech. Rep, (3), 1–56, Spain, 2014.